nature communications

Article

https://doi.org/10.1038/s41467-024-53234-0

Seismic slip channeling along the East Anatolian Fault illuminates long-term supercycle behavior

Received: 16 March 2024

Accepted: 8 October 2024

Published online: 16 October 2024

Check for updates

Andrea Billi[1], Fabio Corbi[1], Marco Cuffaro[1], Barbara Orecchio[2], Mimmo Palano[3], Debora Presti[2] & Cristina Totaro[2]

The two Mw > 7.5 earthquakes that struck the East Anatolian Fault (EAF), Türkiye, in 2023 caused more slip than expected, indicating that they were potentially part of a supercycle, in which the occurrence probability of a large earthquake is determined by accumulated strain rather than time since the last large earthquake. Here, we show two potential supercycles along the EAF, analyzing earthquakes from the last two millennia. Within each supercycle, seismic ruptures originated in the northeast and progressively spread southwestward with an increasing number of earthquakes until a new supercycle began with another large earthquake in the northeast. To understand the supercycle behavior, we analyze the aftershock sequences of the four most recent Mw≥6.1 mainshocks (2010–2023). This series of earthquakes progressed southwestward, characterized by an increasing diversity of focal mechanisms and a heightened dispersion of epicenters across a branched seismotectonic environment. Earthquakes in the northeast exhibit spatial and kinematic channeling along the master fault surface, effectively transferring slip southwestward and there potentially triggering dispersed and heterogeneous earthquakes. This spatiotemporal pattern seems connected with varying levels of a presumably-innate property of fault sections or regions, ruling the process of seismic slip channeling, which could also explain the behavior of long-term supercycles.

Devastating earthquakes continue to surprise and give lessons to scientists, especially when these events exhibit unexpected characteristics[1], such as the 2023 doublet of Mw > 7.5 earthquakes within a day along the same fault system in Türkiye[2–9]. Indeed, several great earthquakes in the past served as scientific watershed episodes. The Mw7.9 San Francisco earthquake of 1906 sparked the development of the elastic rebound theory[10], which is still used to describe the basics of earthquake cycles. Another significant event was the 1964 Alaskan Mw9.2 earthquake with its associated tsunami. The earthquake served as unmistakable proof for the theory of plate tectonics[11], while the tsunami resulted in the establishment of the NOAA Tsunami Warning Center, which has since saved lives in the Pacific region. Between 1939 and 1992, ten Mw ≥ 6.7 earthquakes that progressively unzipped ~1000 km of the North Anatolian Fault, Türkiye, taught geoscientists how secular stressing and static stress transfer after large earthquakes can trigger the next major event along the same fault system[12,13].

Occurrences of temporally and spatially close earthquakes are hence unmissable opportunities to advance our understanding of active fault mechanics and regional hazards[14]. The most recent

[1]Consiglio Nazionale delle Ricerche, IGAG, at Sapienza University of Rome, P.le A. Moro, 5, 00185 Rome, Italy. [2]Dipartimento di Scienze Matematiche e Informatiche, Scienze Fisiche e Scienze della Terra, Messina University, Viale Ferdinando Stagno d'Alcontres, 31, 98166 Messina, Italy. [3]Department of Earth and Marine Sciences, University of Palermo, Via Archirafi 22, 90123 Palermo, Italy. e-mail: andrea.billi@cnr.it

noteworthy instance with a significant impact on people and infrastructure is the aforementioned doublet of Mw > 7.5 earthquakes that occurred along the East Anatolian Fault (EAF)[3,9,15–19].

To improve our knowledge of fault unzipping through multiple earthquakes and hence of seismic supercycles[20], if that is truly the case for the EAF earthquakes[3], we compare the seismotectonic features of the two 2023 mainshock-aftershock sequences near Pazarcık (Mw_{max}7.7) and Elbistan (Mw_{max}7.6), southwestern EAF, with those of the two previous $Mw_{max} \geq 6.1$ sequences, which occurred in 2010 and 2020, respectively, near Kovancılar (Mw_{max}6.1)[21,22] and Elâzığ (Mw_{max}6.8)[23,24] along the northeastern EAF (Fig. 1). To do so, we gathered data mainly from the Türkiye's Disaster and Emergency Management Authority, i.e., the AFAD databases, and from other historical databases (see "Methods"). We then place the four mainshock-aftershock sequences within a multimillennial context of historical seismicity[25] and use them as proxies to interpret long-term earthquake supercycles. The analogy we propose between recent mainshock-aftershock sequences and long-term clusters of earthquakes, or possibly supercycles[20], is based on a concept termed seismic slip channeling. For each investigated earthquake sequence, the degree of seismic slip channeling is calculated by examining some geometric parameters of faults and earthquakes; specifically, the distance between the epicenters of mainshocks or aftershocks and the EAF mapped master surface. This distance is compared, in a two-dimensional diagram, to the angle between azimuths of the EAF master surface and seismic slip vectors obtained from focal mechanisms.

The EAF is a major >600 km long tectonic boundary in eastern Türkiye, separating the Anatolian, Arabian, and Eurasian plates, which come into contact at the Karliova triple junction located at the northeastern tip of the EAF (Fig. 1). The EAF has a general subvertical attitude, NE-SW strike, and left-lateral kinematics[26–28]. It is best defined as a complex and branched strike-slip fault system, which includes a segmented master fault surface, as is mapped on the Earth's surface, and numerous subsidiary faults with different orientations and inclinations. In detail, the tectonic architecture of the EAF appears twisted and accompanied by variously oriented subsidiary faults between the Karliova triple junction and the 2010 Kovancılar mainshock epicenter (Fig. 1). Southwestward, the EAF becomes more linear and narrower where the 2010 Kovancılar and 2020 Elâzığ mainshock epicenters occurred, particularly in the area of the 2020 event. Further southwestward, the EAF becomes progressively more complex from a geometrical point of view, splitting into a few main branches, with fault segments oriented from E-W to N-S[26–28]. The two 2023 mainshocks occurred along two main branches of this southwestern portion of the EAF (Fig. 1).

In the area of the 2023 Pazarcık mainshock (Fig. 1), the EAF trace bends southward from the NE-SW strike to NNE-SSW, forming a releasing bend with an associated extensional basin developed within the general left-lateral kinematics of the entire fault system. The 2023 Pazarcık mainshock nucleated there on the Narlı fault zone and then spread along the EAF master surface, affecting both the Amanos segment to the south and the Pazarcık and Erkenek segments to the north[16,19,29].

The following Mw7.6 Elbistan mainshock originated along an E-W striking segment of the Çardak fault, 95 km to the NNE of the Pazarcık maishock epicenter (Fig. 1), and then spread westward to the Savrun fault and eastward through the Nurhak tectonic complexity, along a minor fault between the Malatya and Sürgu major faults. The Mw7.6 mainshock triggered a series of aftershocks, including normal faulting earthquakes near the Savrun fault. Some aftershocks located to the north of the Çardak fault are compatible with a N-dipping fault[16,19,29].

On a larger scale, all the aforementioned fault segments belong to the broad and complex EAF strike-slip system, in particular the branched southwestern part[26–28]. For the EAF, which is a plate boundary more than 600 km long, it is indeed reasonable to hypothesize a composite fault zone up to a few tens of km thick (<~10% of the fault length), including several fault segments with slip distributed partly on the master fault and partly on subsidiary faults. The 2023 earthquakes demonstrate how complex a subvertical strike-slip plate boundary can be and thus how varied the seismic ruptures and slip propagation along the boundary are[9,30,31]. Fault stepovers as well as releasing and restraining bends or multiple fault segments variously oriented and inclined can partition, facilitate, or restrain the slip propagation along the fault system[32,33]. As this is one of the main focuses of our discussion, below, by using the seismic slip channeling, we aim at assessing such a slip complexity.

To further complicate the general seismotectonic architecture of the EAF, to the south of the 2023 Pazarcık earthquake epicenter, the EAF system joins with the strike-slip Dead Sea Fault system and the Cyprus compressional arc, which are both active plate boundaries of the eastern Mediterranean region[34] (Fig. 1). These boundaries, particularly the Cyprus arc, may influence the seismotectonics of the southwestern section of the EAF as it will be briefly discussed below.

Our aim is to assess the extent to which seismic deformation is directed along or dispersed around the EAF master surface, particularly concerning seismic slip parallel, oblique, or perpendicular to the master surface. To do so, we use the aforementioned seismic slip channeling. Additionally, our goal is to comprehend whether the seismic slip channeling itself is connected with an innate property of fault sections or regions, rather than being influenced by specific earthquake characteristics, such as mainshock magnitude. Below, based on an analysis of earthquakes from the last two thousand years, we identify two possible supercycles along the EAF. Each supercycle began with a major earthquake in the northeast, followed by a southwestward trend in seismic activity. To investigate this pattern, we analyze aftershock sequences from the four most recent $Mw \geq 6.1$ mainshocks (2010–2023), revealing, also in this case, a southwestward trend. This trend was distinguished by increased variability in focal mechanisms and broader epicenter dispersion in a complex seismotectonic setting. In the northeast, seismic activity was concentrated along the master fault, allowing slip to be transferred southwestward and potentially triggering more scattered earthquakes. This observed trend, attributed to a process we describe as seismic slip channeling, may help explain the long-term dynamics of supercycles along the EAF.

Results

Uncertainties and terminology

We acknowledge that our analyses of both recent (Figs. 1–3) and historical (Fig. 4) data are inevitably subject to uncertainties inherent in seismological catalogs. This applies also to the AFAD databases utilized here, which have intrinsic limitations regarding the precise location of instrumental earthquakes and their focal attributes[22,35], as well as the intensity, magnitude, and location of historical earthquakes. However, it is important to acknowledge that the recording of the four recent seismic sequences (2010–2023) studied here benefited from a significant strengthening of the AFAD seismic network since 2007. This enhancement has led to improved detection thresholds and reduced location uncertainties[26,35]. Even though providing quantitative estimates of uncertainties is challenging, approximate estimates from first-order relocations of the four studied sequences indicate horizontal and vertical mean uncertainties around 3 and 4 km, respectively[22,26,30]. At the scale of investigation of the present study, such uncertainty in the epicentral location ensures that the observed differences in the aggregate dataset of our elaborations remain robust. In particular, uncertainty and errors should affect all four aftershock sequences roughly equally without changing the observed patterns.

Concerning the completeness of the AFAD catalog for instrumental earthquakes, many studies indicate a lower threshold of Mw around 3.0 or even less since 2010 in the EAF region[21,26,35,36]. Since our

https://doi.org/10.1038/s41467-024-53234-0

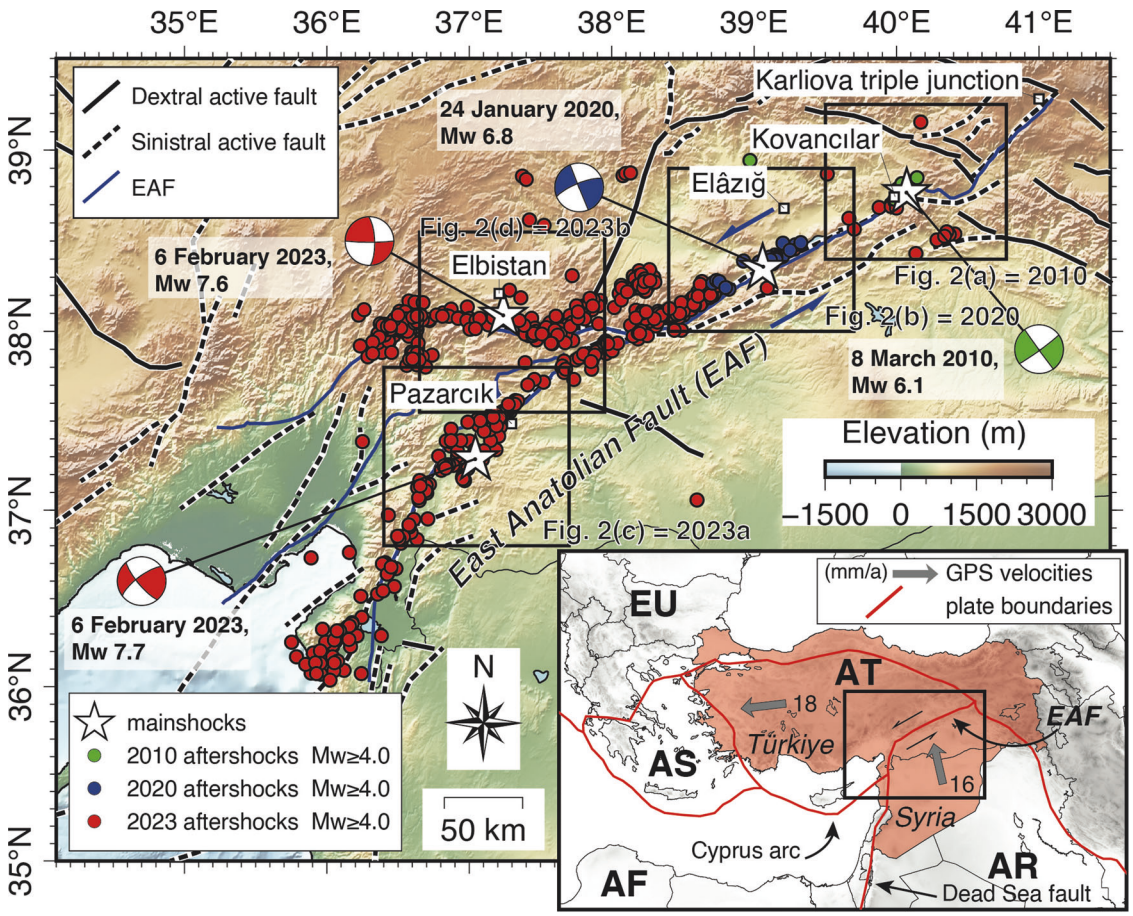

Fig. 1 | Map of the East Anatolian Fault, eastern Türkiye. Green, blue, and red dots indicate earthquake epicenters (Mw ≥ 4.0) from the four mainshock-aftershock sequences studied in this paper along the East Anatolian Fault (EAF), namely, from NE to SW and from older to younger sequences: (green) 2010 Mw_{max}6.1 Kovancılar sequence; (blue) 2020 Mw_{max}6.8 Elâzığ sequence; (red) 2023a Mw_{max}7.7 Pazarcık and 2023b Mw_{max}7.6 Elbistan sequences. Beach balls are the focal mechanisms from the four mainshocks. The aftershock distribution and focal mechanisms are obtained from the Türkiye's Disaster and Emergency Management Authority (AFAD) databases. The trace of the EAF master surface in blue is from previous maps[27,28]. The black solid and dashed lines are the active faults in the study area, reported with the associated kinematics (see legend) as obtained from the European Database of Seismogenic Faults (EDSF13, https://seismofaults.eu/edsf13). The bottom right inset shows a schematic tectonic map of Türkiye and its surroundings. Topography and bathymetry data are from the recent GEBCO_2023 Grid[66]. Tectonic plates with boundaries marked in red are as follows: AF Africa, AR Arabia, AS Aegean Sea, AT Anatolia, and EU Eurasia[67]. Gray arrows with numbers are GPS velocities in mm/a[68] relative to fixed Eurasia. The data shown in this figure and related methods of analysis are reported and explained in the "Methods" and Supplementary Information.

study focuses on earthquakes with Mw ≥ 4.0, we are confident that we are well above the catalog's completeness threshold.

Furthermore, our calculation of seismic slip channeling employed a two-dimensional analysis (Fig. 3), despite the data being distributed in a three-dimensional space. For this reason, as we will explain below, our analysis assumes a subvertical EAF zone.

In this paper, we use the term premainshock to refer to Mw ≥ 4.0 earthquakes that occurred up to six months before one of the four studied mainshocks, within a radius of 50 km around the mainshock epicenter, and with a maximum depth of 25 km. The term aftershock is instead used for Mw ≥ 4.0 earthquakes occurring up to 1 month after one of the four studied mainshocks, within the same spatial parameters as for premainshocks.

Four recent sequences

Figures 1–3 depict seismological data from the four 2010–2023 Mw ≥ 6.1 mainshock-aftershock sequences. In ensemble, the sequences show a northeast-to-southwest migration and progressive seismic unzipping of the EAF[37] (Fig. 1). The 2023 mainshock nodal planes are coaxial (parallel) with the local strikes of the EAF master surfaces, whereas the aftershock focal mechanisms are both geometrically and kinematically noncoaxial or poorly coaxial with the mainshocks and hence also with the local strikes of the EAF master surfaces (Figs. 1 and 2). In particular, attitudes of both nodal planes, slip vectors, and P- and T-axes from the aftershock focal mechanisms display great variability (Fig. 2c, d). In contrast, nodal planes of focal mechanisms from two premainshocks are coaxial with the nodal planes of the 2023 Pazarcık mainshock (Fig. 2c). In both the Pazarcık and Elbistan cases, several aftershock epicenters are located off the EAF master surface, especially in the Pazarcık instance (Fig. 2c, d).

Unlike the 2023 sequences, nodal planes of focal mechanisms from both the premainshocks and the aftershocks of the 2010 (Fig. 2a) and 2020 (Fig. 2b) sequences are geometrically and kinematically coaxial with the nodal planes of the related mainshocks, with corresponding P-axis attitudes that are clustered around the subhorizontal NNE trend, consistent with left-lateral displacements along the NE-SW striking EAF. Slip vectors from focal mechanisms are indeed horizontally clustered along the NE-SW trend and along the orthogonal one. Both in the 2010 sequence and in the 2020 one, most aftershock epicenters are located along and close to the EAF master surface, particularly in the 2020 instance (Fig. 2a, b). The coaxiality of focal

https://doi.org/10.1038/s41467-024-53234-0

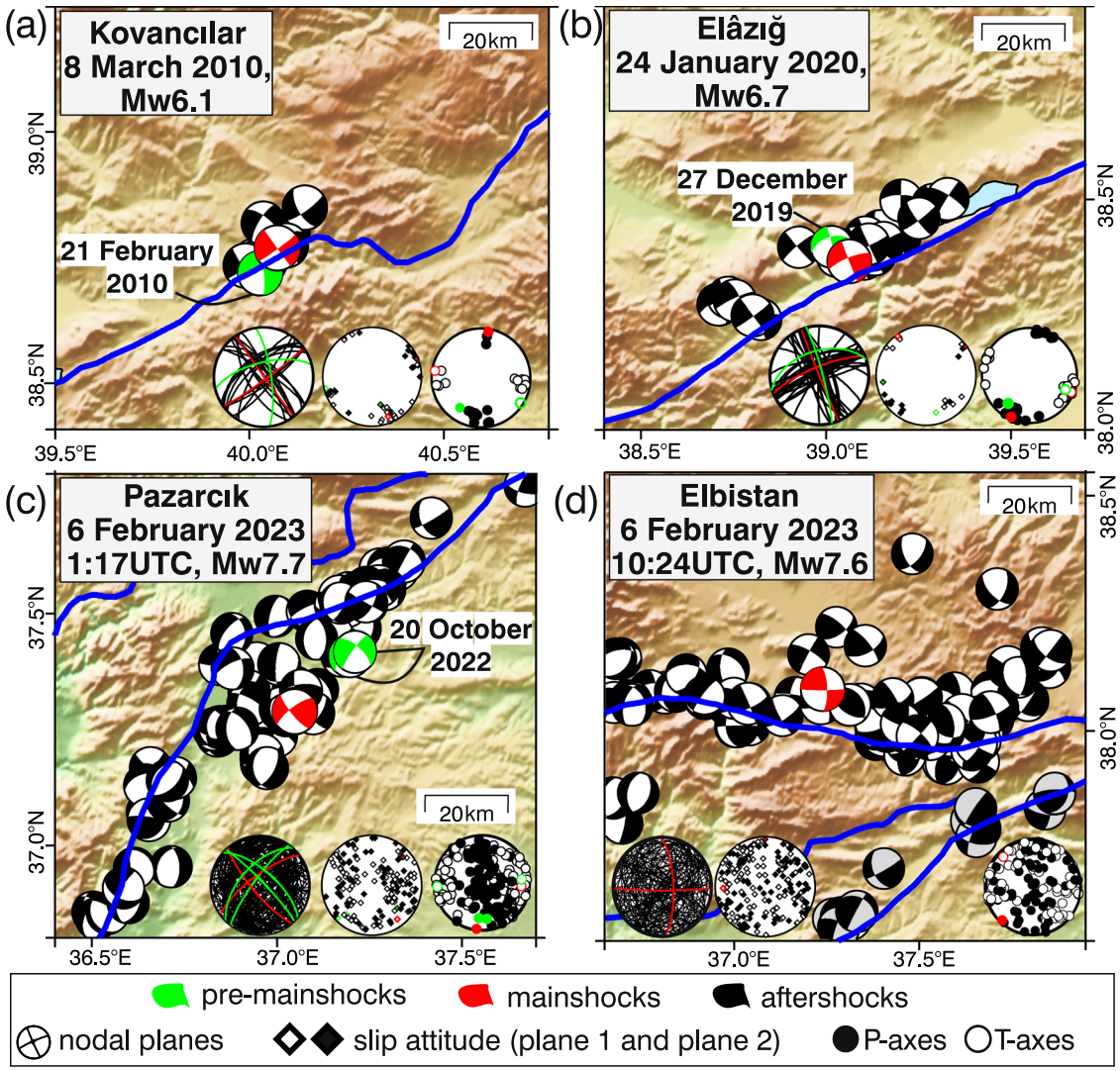

Fig. 2 | Earthquake focal mechanisms. Distribution along the EAF of earthquake focal mechanisms (beach balls, Mw ≥ 4.0) for the four mainshock-aftershock sequences (also including the Mw ≥ 4.0 premainshocks) studied in this paper: **a** 2010 Mw_{max}6.1 Kovancılar sequence; **b** 2020 Mw_{max}6.8 Elâzığ sequence; **c** 2023a Mw_{max}7.7 Pazarcık sequence; and **d** 2023b Mw_{max}7.6 Elbistan sequence. See Fig. 1 for locations of (**a**), (**b**), (**c**), and (**d**) along the EAF. Three stereoplots in each panel show, from left to right, attitudes of nodal planes, seismic slip vectors, and P- and T-axes, respectively, obtained from the focal mechanisms. These plots were made using the GMT software[69]. In (**d**), focal mechanisms with gray background are assumed related to the primary branch of the EAF master surface rather than the northern branch that generated the 2023 Elbistan mainshock; hence, the related data are not included into the stereoplots. For each sequence, premainshocks refer to earthquakes that occurred within six months before each mainshock, whereas aftershocks refer to earthquakes that occurred within one month after the mainshock. Topography and bathymetry data are from the recent GEBCO_2023 Grid[66]. The data shown in this figure and related methods of analysis are reported and explained in the "Methods" and Supplementary Information.

mechanisms with respect to the EAF master surface is quantitatively described below (Fig. 3).

Seismic slip channeling

The four studied mainshock-aftershock sequences are hence heterogeneous in terms of slipping surface attitude and kinematics, as well as the epicenter locations with respect to the EAF master surface (Fig. 2). To evaluate all these parameters together, we develop the aforementioned concept of seismic slip channeling (Fig. 3), which expresses whether seismic slip is channeled along (close to) the master fault with a movement coaxial (parallel) to it, as determined by the focal mechanisms. Thus, the concept is directly related to the efficiency of the seismic displacement translation along and parallel to the master fault itself and establishes a bridge between seismological data and surface tectonics, i.e., the EAF mapped master surface. A pioneer study on this theme along the EAF was realized in 1991[38].

Assuming a nearly vertical attitude of the EAF strike-slip system[26], we plotted the distance between earthquake epicenters and the EAF mapped master surface (i.e., the nearest main trace from each epicenter) against the small azimuthal angle between the local master surface itself and the seismic slip vectors derived from the focal mechanisms (Fig. 3 and Supplementary Fig. 1; "Methods" and Supplementary Information). In the same diagrams, with conventional color codes[39], we also plotted the earthquake kinematics derived from the focal mechanisms. Last, since the amount of seismic slip is directly related to the earthquake magnitude, we represented this latter attribute through different marker sizes (Fig. 3). For the azimuth of the EAF mapped master surface, we utilize the mapping provided by previous studies[27,28]. As mentioned above, earthquake epicenters and seismic slip data are sourced from the instrumental seismicity catalog within the AFAD databases ("Methods", Supplementary Information, Supplementary Figs. 1 and 2, Supplementary Tables 1–3, and Supplementary Data 1).

https://doi.org/10.1038/s41467-024-53234-0

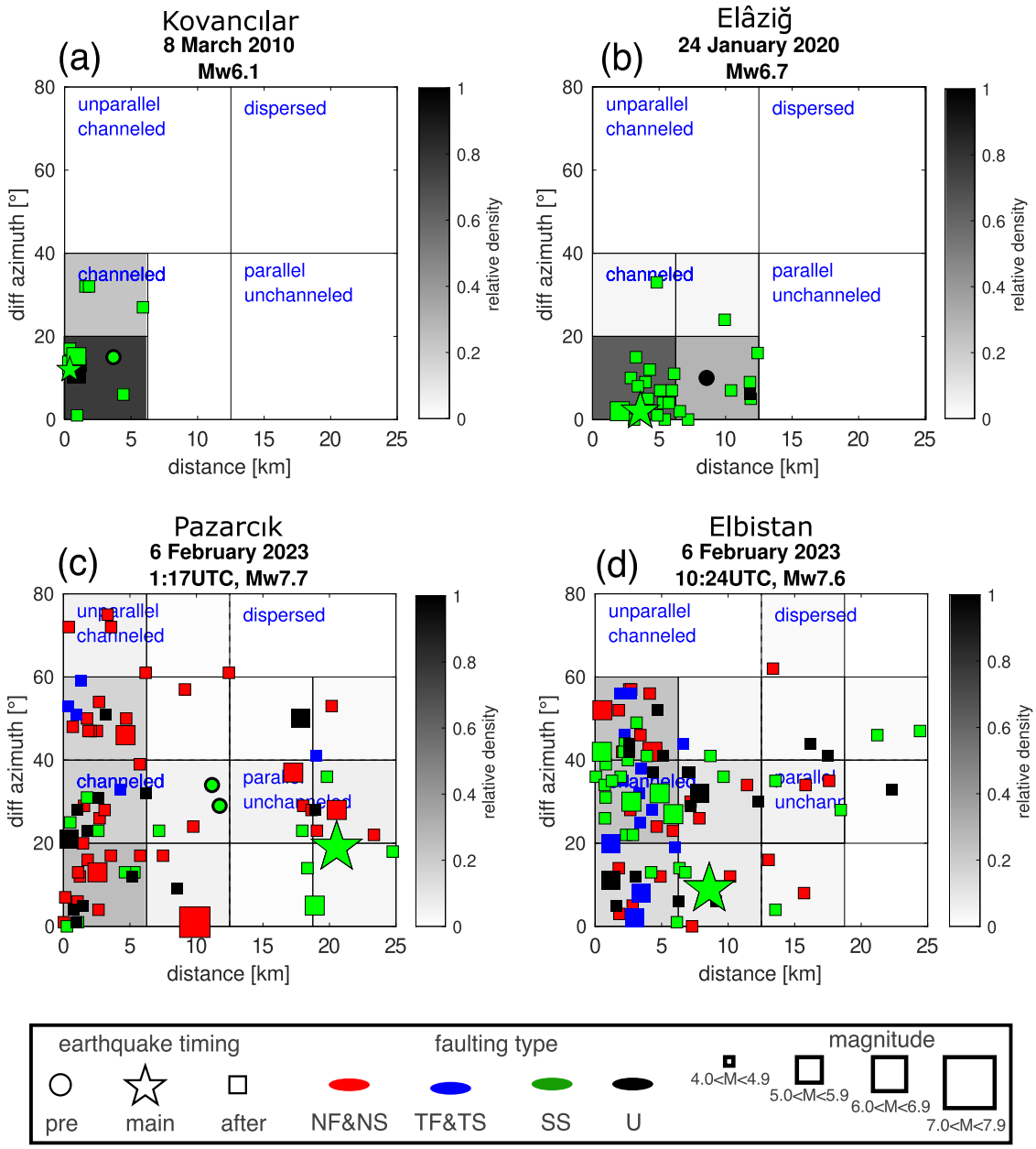

Fig. 3 | Seismic slip channeling along the East Anatolian Fault. a 2010 Mw_{max}6.1 Kovancılar sequence. **b** 2020 Mw_{max}6.8 Elâzığ sequence. **c** 2023a Mw_{max}7.7 Pazarcık sequence. **d** 2023b Mw_{max}7.6 Elbistan sequence. Seismic slip channeling expresses whether seismic slip is channeled along and near the master fault surface with a movement coaxial (parallel) to it, as determined by the focal mechanisms. In each diagram, the earthquakes (Mw ≥ 4.0) shown in Fig. 2 are projected according to the orthogonal distance between each earthquake epicenter and the mapped EAF master surface (abscissa axis) against the small azimuthal angle between the local master surface itself and the seismic slip (ordinate axis), which is derived from the focal mechanisms. The four diagrams represent the four mainshock-aftershock sequences (including also some premainshocks) studied in this paper (same as Fig. 2). Each diagram is divided into four arbitrary major fields, based on data distribution, representing various degrees of seismic slip channeling: channeled, dispersed, parallel unchanneled, and unparallel channeled. Gray shading in square bins is the relative density of data (number of events in each bin normalized by total number of events of each sequence). Earthquake timing: pre is a premainshock (up to 6 months before the mainshock), main is a mainshock, and after is an aftershock (up to one month after the mainshock). Conventional faulting type[39]: red is normal faulting (NF) or normal faulting with a minor strike-slip component (NS); blue is thrust faulting (TF) or thrust faulting with a minor strike-slip component (TS); green is strike-slip faulting (SS); and black (U) is unclassified kinematics. The data shown in this figure and related methods of analysis are reported and explained in the "Methods" and Supplementary Information. See Supplementary Figs. 1 and 2 for further information.

The main aim of the seismic slip channeling analysis is to render the geometric-kinematic complexity of mainshock-aftershock sequences[9,16,29] in a graphic manner (Fig. 3), which shall be both easily comparable from sequence to sequence and analyzable with statistical methods (Fig. 3 and Supplementary Fig. 2). Each diagram of Fig. 3 is divided into four major fields that represent various gradations of seismic slip channeling: channeled, dispersed, parallel unchanneled, and unparallel channeled. The boundaries between different fields have been set arbitrarily based on data distributions. The two end-members are channeled slip, i.e., seismic slip parallel and close to the master fault, and dispersed slip, i.e., seismic slip unparallel to and off the master fault. The gray shading of each bin in Fig. 3, which includes a total of 16 square bins for each panel, represents the density distribution of events on the diagram plane, i.e., the number of events in

https://doi.org/10.1038/s41467-024-53234-0

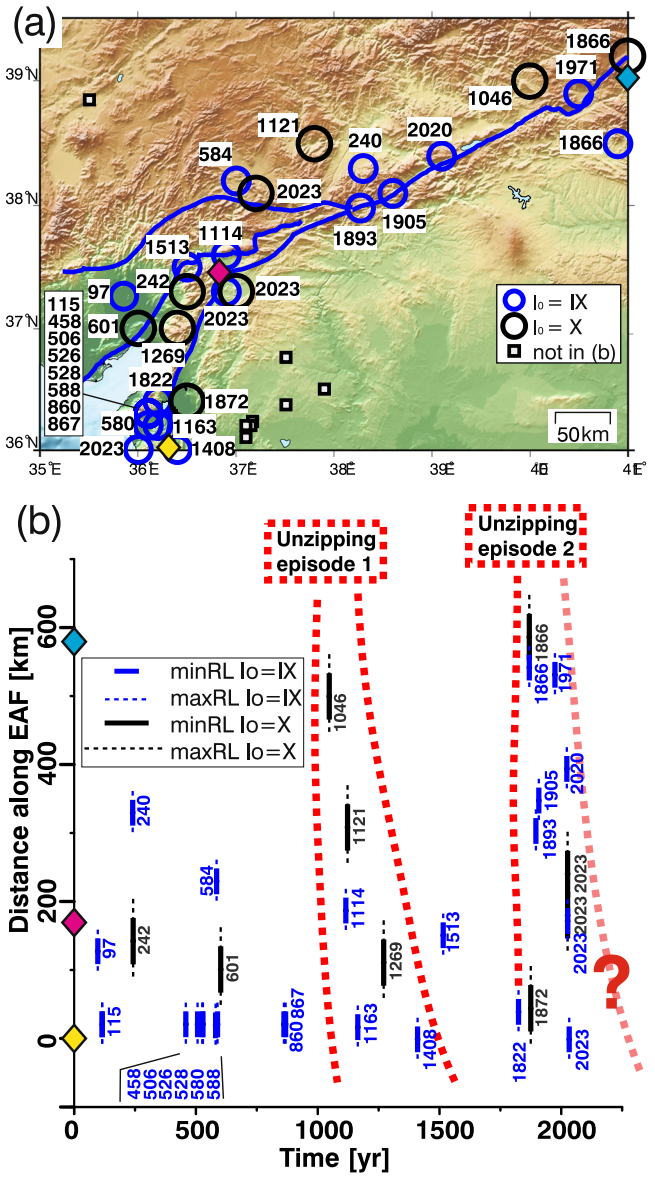

Fig. 4 | Spatiotemporal distribution of historical and recent earthquakes along the East Anatolian Fault. Spatial and temporal distribution of destructive earthquakes ($I_0 \geq$ IX and Mw ≥ 6.5) occurring between A.D. 1 and 2023 along the EAF. **a** Map of the EAF (same as Fig. 1) showing the epicentral distribution of historical and recent earthquakes (black numbers are A.D. years of the earthquakes). Squares indicate earthquakes falling in the map area but not included in diagram (**b**). Topography and bathymetry data are from the recent GEBCO_2023 Grid[66]. **b** Earthquake recurrence diagram[20] (distance along the EAF vs. time), showing its rupture history since A.D. 1. For each earthquake, solid and dashed segments indicate the minimum and maximum subsurface rupture lengths estimated for the related magnitude range, respectively (see legend). In particular, we obtained rupture lengths (RL) ranging between 30 (minimum RL for intensity IX) and 60 km (maximum RL for intensity IX), and between 60 (minimum RL for intensity X) and 180 km (maximum RL for intensity X), respectively (see legend). These estimated lengths were plotted in (**b**) consistently with their time-space distribution along the EAF. Dashed red lines are arbitrary indications of two main unzipping episodes during approximately the last 1000 years. The light red dashed line together with the question mark indicates that the unzipping episode 2 could represent a shorter time interval than episode 1. Alternatively, episode 2 could be incomplete and therefore ongoing. Three colored diamonds in (**a**) and (**b**) are spatial markers. Data shown in this figure and related methods of analysis are reported and explained in the "Methods" and Supplementary Information.

each bin normalized by the total number of events of each sequence (Supplementary Fig. 2).

The 2010 and 2020 mainshock-aftershock sequences primarily comprise strike-slip channeled earthquakes that are thus kinematically coaxial with the master fault and close to it, particularly the 2020 sequence (Fig. 3a, b). In these two cases, the maximum density levels are relatively high (0.77 and 0.62 for the 2010 and 2020 sequences, respectively; Supplementary Fig. 2a, b) and fall in the most channeled bin. The two 2023 mainshock-aftershock sequences (Fig. 3c, d), instead, include earthquakes up to a few tens of km away from the master fault and characterized by strike-slip to normal-slip kinematics as well as some thrust-slip events. Indeed, these earthquakes only partially fall within the channeled field, spreading toward the other three fields, particularly for the 2023 Pazarcık sequence. While the maximum density levels also fall within the channeled field, they have lower values compared to the 2010 and 2020 sequences (0.24 and 0.27 for the Elbistan and Pazarcık sequences, respectively; Supplementary Fig. 2c, d). It is critical to note that in the two 2023 cases, aftershocks with extensional and reverse kinematics, which are significantly misaligned with the master fault and the mainshocks, occurred not only in the quadrants farthest from the master fault but also in the nearest ones (Fig. 3c, d). In contrast, in the 2010 and 2020 sequences—particularly the 2020 sequence—the azimuthal alignment between the aftershock slips and both the master fault and the mainshock slip is very pronounced, with an azimuthal distance generally less than 20° regardless of the distance from the master fault (Fig. 3a, b). In all four cases, no systematic patterns are detectable for the earthquake magnitude (Fig. 3).

In synthesis, based on the assumption that the master fault is the structure best capable of transferring (seismic) slip, Fig. 3 helps us determine how many earthquakes occurred along (or inversely far from) the master surface, particularly with slip parallel to the master surface itself. In other words, the figure illustrates how much seismic slip was transferred or diffused in these specific events, either over a narrow fault zone or a wider deformation area, respectively.

Earthquake supercycles

To analyze the time-space pattern of past destructive earthquakes along the EAF and frame the recent mainshock-aftershock sequences within a historical perspective, we built a diagram previously used to identify earthquake supercycles elsewhere[20,40]. We plotted the spatial and temporal distributions of destructive earthquakes ($I_0 \geq$ IX and Mw ≥ 6.5) occurring between A.D. 1 and 2023 along the EAF (Fig. 4). Being a time-line representation, this diagram (Fig. 4b) compresses the fault-epicenter information along the EAF master surface. Uncertainties and limits of the historical source material are reported above and in the historical catalogs[41–43]. In Fig. 4b, the uncertainty associated with the coseismic rupture lengths is represented by dashed lines. Moreover, we acknowledge that a large supercycle with a return period of ~900 years along the EAF was recently proposed[9] and a general spatiotemporal southwestward migration of recent and past seismicity was previously documented[37].

With triangular-shaped clusters of earthquakes, Fig. 4b shows three major earthquake-rich periods, ranging from A.D. 240 to 601 (or perhaps even 867), 1046 to 1408, and 1866 to 2023. At least for the two youngest and more complete periods, named unzipping episodes 1 and 2 in Fig. 4b, we observe a marked tendency of earthquake migration from northeast to southwest along the EAF, such that one or a few earthquakes in the northeast are followed by clusters of earthquakes toward the southwest, likely mirroring the EAF southwestern branched pattern (Fig. 4). The A.D. 1046 and 1866 earthquakes constitute the apices to the northeast of the two clusters, which tendentially evolve over time toward the southwest, where a greater number of earthquakes occur than toward the northeast. Within these clusters, there are also seismic episodes, such as that from A.D. 1114 to 1121 or that

from 1872 to 1971, with migration in the opposite direction (northeastward) from the predominant one toward the southwest, thus testifying a predominant but non-unique tendency for earthquakes to migrate toward the southwest along the EAF (Fig. 4).

Discussion

Seismic slip channeling and mainshock magnitude

To investigate the causes of the varying degrees of seismic slip channeling along the EAF (Fig. 3), we propose a null hypothesis that these degrees are inversely proportional to the Mw_{max} of the mainshock-aftershock sequences. Essentially, higher seismic energy levels might activate a greater number of fault segments, including those located far from the mainshock epicenter, due to elastic stress transfer[44–46]. This hypothesis is supported by the observed decrease in seismic slip channeling and a concurrent increase in Mw_{max} for the four studied sequences progressing southwestward along the EAF (Figs. 1–3). Additionally, this hypothesis correlates with the observation that larger earthquakes typically result in longer and wider seismic ruptures[47], potentially triggering aftershocks from critically stressed faults with different dips and strikes. Hence, the null hypothesis could explain the variability in nodal plane attitudes and the decreased seismic slip channeling observed in high Mw_{max} mainshock-aftershock sequences along the EAF (Figs. 1–3).

However, at least one of our key observations appears to contradict the null hypothesis. For the 2010 and 2020 sequences, there is clear parallelism between the seismic slips and the closest master fault, regardless of the aftershock distance to the master fault itself (Fig. 3a, b). Conversely, the lack of parallelism in the 2023 sequences is also evident, independent of the aftershock distance to the nearest master fault (Fig. 3c, d). From this observation, it becomes apparent that the fault zone segments that hosted the 2010 and 2020 earthquakes differ in tectonic texture from those that hosted the 2023 earthquakes. The segments activated during the 2023 events appear to be tectonically more heterogeneous than those activated during the 2010 and 2020 events. This contrast suggests that seismic slip channeling is not predominantly or exclusively governed by the magnitude of the mainshocks.

An innate property of fault segments?

The discussion above suggests that the process of seismic slip channeling may be connected with an innate property of the fault or fault segments, such as the tectonic texture, rather than being solely dependent on specific earthquake characteristics such as mainshock magnitude. As mentioned above, we note that while generally larger earthquakes can activate aftershocks over a wider area, thereby involving more diverse fault planes, in the two 2023 instances, the diversity in azimuth and mechanism is just as evident among aftershocks very close to the master fault rupture (Fig. 3c, d). This supports the idea that the southwest section of the EAF is inherently prone to poor channeling compared to the northeast section. In other words, we contend that Mw_{max} alone cannot fully explain the varying levels of seismic slip channeling observed along the EAF and, more broadly, the seismic behavior of long fault zones. While there appears to be a direct relationship between Mw_{max} and seismic slip channeling based on the results shown in Fig. 3, we hypothesize that the degree of seismic slip channeling is not merely a matter of the quantity of energy released by the earthquake. It should also involve how this energy is stored segment by segment before being seismically dissipated over a large or limited number of discontinuities in the rock volume, indicating fault zone maturity[48]. Indeed, the number, spatial distribution, and orientation of the surfaces of weakness (i.e., the tectonic texture) capable of dissipating seismic energy through slip must play a fundamental role in seismic slip channeling. There must be a complex trade-off between the released seismic energy and the fault system's ability to accommodate it across single mature versus numerous immature fault segments[48,49].

If seismic slip channeling is at least partially connected with an innate property of faults or fault segments, then hypotheses related to rock rheology and fault maturity can be advanced to explain the observed seismic slip channeling. Recent natural data and laboratory experiments have demonstrated how variations in rheology over crustal volumes surrounding a seismic fault can influence the dispersion of seismic slip[50]. Specifically, ductile crustal rheology can lead to distributed seismicity, which follows different scaling laws compared to seismicity occurring on fault volumes exhibiting elasto-frictional stick-slip behavior[50]. In the case of the EAF, the shallowing of the Moho depth, reduced Vp/Vs ratio, and high heat flux values toward the southwest[51] may indicate a crustal rheology change in that direction, potentially resulting in a dispersed fault architecture (Fig. 1) and related dispersion of seismicity (Figs. 2–4). If so, interaction between fault slip and off-fault plasticity may lead to rupture arrest and spatiotemporal clustering of seismicity[52], thus explaining the spatiotemporal pattern of historical earthquakes along the EAF and its hypothetical supercycle behavior (Fig. 4). Plasticity may also lead to irregular patterns of seismicity with partial ruptures spreading over the fault system[53,54], thus explaining the complex rupture pattern of the 2023 earthquakes along the EAF (Fig. 2).

However, a lack of detailed information on the bulk rheology of the rocks encompassing the southwestern portion of the EAF prevents further speculation on this theme. Additionally, or alternatively, the junction, toward the southwest, of the EAF with the strike-slip Dead Sea Fault system and the nearly orthogonal intersection with the Cyprus compressional arc (Fig. 1) could act as barriers to efficient southward slip transfer along the EAF, potentially influencing its seismicity and structural architecture.

Fault segment maturity, directly correlated with slip history and fault longevity, may significantly affect earthquake characteristics such as slip distribution and the number of ruptured segments. Less mature segments often exhibit a broader distribution of seismic slip and a larger number of ruptured segments[48,55,56]. Accordingly, the EAF segments where the 2010 and 2020 mainshocks occurred (channeled seismic slip; Fig. 3a, b) might be interpreted as more mature than the southwestern segments where the 2023 mainshocks occurred (poorly channeled seismic slip; Fig. 3c, d). It is worth noting that fault segments can vary in maturity along their propagation direction, with mature overall faults containing immature segments[48,57]. Furthermore, immature fault segments associated with diffuse fracture networks may host large earthquakes, while smaller earthquakes may occur in mature systems[48]. Laboratory experiments also support an inverse correlation between off-fault deformation and fault maturity[58,59]. Consequently, well-channeled seismic slip (Fig. 3) might indicate fault segment maturity[48] and its capacity to promptly dissipate stored strain through seismic and possibly aseismic slip. Conversely, poorly channeled seismic slip may suggest less mature fault systems, which are less capable of promptly dissipating tectonic strain, thus leading to bursts of seismic ruptures, as observed in 2023 along the southwestern branches of the EAF[3,9]. However, considering the aforementioned points about seismicity and fault maturity, we must acknowledge that using seismic slip channeling to determine fault seismological maturity, or vice versa, is currently largely hypothetical. Nonetheless, we propose a plausible link that might open up an avenue of inquiry, bridging the seismic behavior and structural architecture or tectonic texture of active fault zones[48].

We also acknowledge that, at least for the case of the 2023 Pazarcık sequence, the poorly channeled seismic slip (Fig. 3c) could be explained by certain features of the specific earthquake ruptures described above, namely the initiation of the Pazarcik earthquake on the Narlı fault and the potential northward dip of the Çardak fault.

While the aftershocks along the Narlı fault are indeed far from the EAF master surface, they are very close to the specific fault rupture of the 2023 mainshock, which includes the Narlı fault itself. Similarly, for what concerns the Çardak fault, if it dips to the north, then the aftershocks there may not actually be far from the master fault plane. However, in our view, seismic slip channeling should serve as a synthetic representation of this seismic rupture complexity and hence the tectonic texture complexity (see the Tectonic Setting section), as for the Pazarcık sequence (Fig. 3c).

Seismic slip channeling and earthquake supercycles

Drawing from previous studies on similar spatiotemporal earthquake distributions (Fig. 4)[20,40,44], we might tentatively interpret the two youngest seismic clusters depicted in Fig. 4b as earthquake supercycles, as has been partially done previously along the EAF[9]. However, the crux of our scientific inquiry here lies not in the mere classification of seismic events, but rather in the observation that seismic activity along the EAF comprises clusters, as previously noted[41]. Moreover, these clusters exhibit a distinct space-time pattern characterized by a progressive migration from northeast to southwest[9], accompanied by a parallel increase in the number of earthquakes over a branching fault pattern (Fig. 4).

A plausible mechanism accounting for this evidence could be the efficiency of slip transfer, as elucidated by the seismic slip channeling analysis (Fig. 3). This is particularly relevant if we consider the hypothesis that seismic slip channeling is substantially connected with an innate property of the various fault segments. Accordingly, where slip is spatially channeled along the master fault surface and kinematically aligned with it, we may hypothesize that the overall fault slip amount could be readily accommodated not only by earthquakes but also by some aseismic motion, thanks to the slip-favorable tectonic texture. Conversely, in regions where slip is dispersed and kinematically poorly aligned with the master fault surface, occasional seismic activity rather than continuous aseismic motion primarily accommodates slip over a broader area encompassing multiple fault segments (Figs. 2 and 3).

In other words, where the fault's ability to accommodate slip (channeled slip) increases (Fig. 3), both seismic and aseismic slip can be reasonably expected along the master fault itself. The hypothesized ability of channeled fault segments in the northeastern EAF to accommodate aseismic slip in addition to seismic slip could explain our initial observation: i.e., the two Mw>7.5 earthquakes that struck the EAF in 2023 caused more slip than expected[3]. The deficit of seismic slip toward the northeastern sectors of the EAF could, in fact, be compensated by some aseismic slip, thus potentially explaining how earthquake supercycles work along the EAF; however, the topic of aseismic movement is beyond the scope of this paper and remains to be investigated in detail in the future.

Our findings elucidate the process of progressive seismic unzipping along the EAF, characterized by the spatial and temporal migration of seismicity toward the southwest, accompanied by dispersion and an increasing number of earthquakes, transitioning from channeled to dispersed seismic slip. The collective behavior of four recent mainshock-aftershock sequences along the EAF (Figs. 1–3) might be illustrative of its longer-term behavior (Fig. 4). The implication is that well-channeled seismic slip in the northeastern section of the EAF, perhaps coupled with some aseismic slip, would appear capable of triggering bursts of earthquakes toward the southwestern section of the fault, leading to an extended period of heightened seismic hazard. Moving forward, it is imperative to ascertain whether the seismic behavior observed along the EAF in this study is typical elsewhere and whether seismic slip channeling and earthquake supercycles are causally linked, particularly in regions where supercycles have been documented or hypothesized[60–63]. Therefore, to advance our comprehension of earthquake occurrences beyond individual events, the next step entails examining seismic slip channeling in other regions and elucidating its underlying causes.

Methods

Instrumental earthquakes

For instrumental earthquakes (Figs. 1–4), we used the AFAD database. The selection of this database was guided by two primary criteria: territorial relevance and past experience.

Territorial Relevance: there is a general preference for national seismic catalogs when studying earthquakes within a specific territory. These catalogs are indeed tailored to the region, utilizing seismic networks that are specifically designed and calibrated for better detection and analysis of local earthquakes. Consequently, the AFAD database, being the national seismic catalog, was deemed most appropriate for our study.

Past Experience: in conducting this research, we reviewed recent and past articles on the same seismic sequences to determine which catalogs were used and the outcomes they provided. For the four seismic sequences analyzed in this manuscript, numerous significant articles have utilized the AFAD catalog (refer to citations within this paper). This extensive prior use underscores the reliability and relevance of the AFAD database for our research.

Moreover, the AFAD database uniquely encompasses all the necessary information for our study, including catalogs of focal mechanisms, instrumental earthquakes, and historical earthquakes. Ensuring data homogeneity is crucial, and the AFAD catalog was the only source that provided comprehensive and consistent data across all required parameters. For these reasons, we selected the AFAD database for our instrumental seismological analyses.

Historical earthquakes

For historical earthquakes (Fig. 4 that also includes some instrumental earthquakes), we used various databases (see below). Diagrams of Fig. 4 are inspired by previous works on earthquake supercycles[20,40,60–63]. The spatial and temporal distribution of destructive earthquakes ($I_0 \geq$ IX and Mw ≥ 6.5) occurring between A.D. 1 and 2023 along the EAF was obtained merging data from the following databases: AFAD-Historical Earthquakes (2000 B.C.–1900 A.D., https://deprem.afad.gov.tr/event-historical); CFTI5Med-Catalogo dei Forti Terremoti in Italia (461 a.C.–1997) e nell'area Mediterranea (760 a.C.–1500; https://storing.ingv.it/cfti/cfti5/)[42]; GHEA-Global Historical Earthquake Archive (https://www.emidius.eu/GEH/map.php); AFAD-Instrumental Earthquakes Catalog (1900–Present M ≥ 4.0, https://deprem.afad.gov.tr/event-instrumental). We preferred to consider only destructive earthquakes, thus making the catalog as homogeneous as possible throughout the entire time span (A.D. 1–2023).

To build the diagrams of Fig. 4, we performed an analysis of the space-time rupture history of the EAF for the last ~2000 years, using the aforementioned earthquake databases for information about time of occurrence and intensity (Supplementary Table 3). On the basis of standard magnitude-intensity relationships, we associated (i) to intensity IX the magnitude range 6.5–6.9 and (ii) to intensity X the magnitude range 7–7.5. In particular, consistently with the EAF kinematics, to constrain the length of individual subsurface ruptures, we used the earthquake magnitude-rupture length scaling properly proposed for strike-slip earthquakes[47]. Obviously, in the case of recent earthquakes, these lengths, retrieved from empirical relationships[47], may differ from the lengths measured with seismological or other modern methods. Based on the aforementioned magnitude ranges (i.e., 6.5–6.9 and 7–7.5), we obtained rupture lengths (RL) ranging between 30 (minimum RL for intensity IX) and 60 km (maximum RL for intensity IX), and between 60 (minimum RL for intensity X) and 120 km (maximum RL for intensity X), respectively. This is represented in the legend of Fig. 4 and provides a graphic representation of the uncertainty of the related data. These

estimated lengths are plotted in (b) consistently with their time-space distribution along the EAF.

Seismic slip channeling appraisal

We elaborated the seismic slip channeling diagrams of Fig. 3 as follows. Distance (km) along the abscissa axes is the orthogonal distance between each earthquake epicenter (earthquakes of Fig. 2) and the local EAF master surface (i.e., projecting each earthquake epicenter onto the nearest EAF segment along the line orthogonal to the EAF segment itself). Coordinates of earthquake epicenters are in Supplementary Table 2 and are obtained from the AFAD database (https://deprem.afad.gov.tr/event-focal-mechanism) whereas digital tracks of the EAF segments with related coordinates are available in the Supplementary Data 1 and are obtained from previous maps[27,28]. Distances plotted in the abscissa axes are in Supplementary Table 2.

Differential azimuth (°) is the small azimuthal angle between the local master surface itself and the seismic slip, this latter derived from the focal mechanisms using the WinTensor software[64]. Note that two seismic slip vectors can be retrieved from each focal mechanism. For the differential azimuth in these diagrams (Fig. 3), we considered the slip vector (of the two possible ones in each focal mechanism) minimizing the azimuthal difference (in degrees) with the local azimuth of the EAF master surface. Azimuths of seismic slip and EAF are in Supplementary Table 2 and are obtained, respectively, from the focal mechanisms (AFAD database; https://deprem.afad.gov.tr/event-focal-mechanism) and from previous maps of the EAF[27,28] (see also Supplementary Data 1). Further technical information on the realization of Fig. 3 is provided together with Supplementary Fig. 1.

The gray shading of each bin in the figure, which includes a total of 16 square bins for each panel, represents the density distribution of events on the diagram plane, i.e., the number of events in each bin normalized by the total number of events of each sequence. Density values are displayed in Supplementary Fig. 2.

Data availability

All data used in this work are available both in the Supplementary Information and in a public data repository[65]. In particular: Instrumental seismological data were obtained from the Türkiye's Disaster and Emergency Management Authority AFAD and are available at https://deprem.afad.gov.tr/event-catalog or in Supplementary Tables 1 and 2. Historical seismological data were obtained from four catalogs: AFAD-Historical Earthquakes (2000 B.C.–1900 A.D.) available at https://deprem.afad.gov.tr/event-historical; CFTI5Med-Catalogo dei Forti Terremoti in Italia (461 a.C.–1997) e nell'area Mediterranea (760 a.C.–1500)[42] available at https://storing.ingv.it/cfti/cfti5/; GHEA-Global Historical Earthquake Archive, available at https://www.emidius.eu/GEH/map.php; and AFAD-Instrumental Earthquakes Catalog (1900–Present $M \geq 4.0$), available at https://deprem.afad.gov.tr/event-instrumental. The historical seismological data used in Fig. 4 are available in Supplementary Table 3. In Figs. 1, 2, and 4 and in Supplementary Fig. 1, the trace of the East Anatolian Fault was digitized from maps in previous papers[27,28]. These data are available in Supplementary Data 1. In Figs. 1, 2, and 4 and in Supplementary Fig. 1, topography/bathymetry of maps is obtained from GEBCO[66], and are available at https://www.gebco.net/. In Fig. 1, fault traces (in addition to the EAF drawn from previous maps[27,28]) were obtained from the European Database of Seismogenic Faults, and are available at https://seismofaults.eu/edsf13, where data are distributed under Creative Commons Attribution 4.0 International (CC BY 4.0). In Fig. 1, plate boundaries were obtained from the MORVEL plate motion model obtained from a previous paper[67] and are available at http://www.geology.wisc.edu/~chuck/MORVEL/. In Fig. 1, linear velocities in mm/a of the Anatolia and Arabia plates with respect to the fixed Eurasia plate were computed with the geodetic Euler vectors of a previous paper[68]. Correspondence and requests for materials should be addressed to Andrea Billi, although all data are publicly available online[65] and in the Supplementary Information. No further data were used.

References

1. Wang, K. Megathrust surprises. *Nat. Geosci.* **6**, 11–12 (2013).
2. Abdelmeguid, M. et al. Dynamics of episodic supershear in the 2023 M7.8 Kahramanmaraş/Pazarcik earthquake, revealed by near-field records and computational modeling. *Commun. Earth Environ.* **4**, 456 (2023).
3. Dal Zilio, L. & Ampuero, J. P. Earthquake doublet in Turkey and Syria. *Commun. Earth Environ.* **4**, 71 (2023).
4. Jia, Z. et al. The complex dynamics of the 2023 Kahramanmaras, Turkey, Mw 7.8-7.7 earthquake doublet. *Science* **381**, 985–990 (2023).
5. Karabacak, V. et al. The 2023 Pazarcık (Kahramanmaraş, Türkiye) earthquake (Mw 7.7): implications for surface rupture dynamics along the East Anatolian Fault Zone. *J. Geol. Soc.* **180**, jgs2023–020 (2023).
6. Karabulut, H. et al. Long silence on the East Anatolian Fault Zone (Southern Turkey) ends with devastating double earthquakes (6 February 2023) over a seismic gap: implications for the seismic potential in the Eastern Mediterranean region. *J. Geol. Soc.* **180**, jgs2023-021 (2023).
7. Okuwaki, R. et al. Multi-scale rupture growth with alternating directions in a complex fault network during the 2023 south-eastern Türkiye and Syria earthquake doublet. *Geophys. Res. Lett.* **50**, e2023GL103480 (2023).
8. Över, S., Demirci, A. & Özden, S. Tectonic implications of the February 2023 Earthquakes (Mw7.7, 7.6 and 6.3) in south-eastern Türkiye. *Tectonophysics* **866**, 230058 (2023).
9. Xu, L. et al. The 2023 Mw7.8 Kahramanmaraş, Turkey earthquake: a multi-segment rupture in a millennium supercycle. *Commun. Earth Environ.* **4**, 379 (2023).
10. Reid, H. F. *The Mechanics of the Earthquake, The California Earthquake of April 18, 1906. Report of the State Investigation Commission* 2 (Carnegie Institution of Washington, 1910).
11. Plafker, G. Tectonic deformation associated with the 1964 Alaska earthquake. *Science* **148**, 1675–1687 (1965).
12. Stein, R. S. The role of stress transfer in earthquake occurrence. *Nature* **402**, 605–609 (1999).
13. Şengör, A. M. C. et al. The North Anatolian Fault: a new look. *Annu. Rev. Earth Planet. Sci.* **33**, 37–112 (2005).
14. Galli, P. Nearly simultaneous pairs and triplets of historical destructive earthquakes with distant epicenters in the Italian Apennines. *Seismol. Res. Lett.* **20**, 1–9 (2023).
15. Özkan, A. et al. Characterization of the co-seismic pattern and slip distribution of the February 06, 2023, Kahramanmaraş (Turkey) earthquakes (Mw 7.7 and Mw 7.6) with a dense GNSS network. *Tectonophysics* **866**, 230041 (2023).
16. Barbot, S. et al. Slip distribution of the February 6, 2023 Mw 7.8 and Mw 7.6, Kahramanmaraş, Turkey earthquake sequence in the East Anatolian Fault Zone. *Seismica* https://doi.org/10.26443/seismica.v2i3.502 (2023).
17. Goldberg, D. E. et al. Rapid characterization of the February 2023 Kahramanmaraş, Türkiye, earthquake sequence. *Seismic Rec.* **3**, 156–167 (2023).
18. Kwiatek, G. et al. Months-long seismicity transients preceding the 2023 Mw 7.8 Kahramanmaraş earthquake, Türkiye. *Nat. Commun.* **14**, 7534 (2023).
19. Zhang, Y. et al. Geometric controls on cascading rupture of the 2023 Kahramanmaraş earthquake doublet. *Nat. Geosci.* **16**, 1054–1060 (2023).
20. Philibosian, B. & Meltzner, A. J. Segmentation and supercycles: a catalog of earthquake rupture patterns from the Sumatran Sunda

Megathrust and other well-studied faults worldwide. *Quat. Sci. Rev.* **241**, 106390 (2020).
21. Bulut, F. et al. The East Anatolian Fault Zone: seismotectonic setting and spatiotemporal characteristics of seismicity based on precise earthquake locations. *J. Geophys. Res.* **117**, B07304 (2012).
22. Tan, O. et al. Aftershock study and seismotectonic implications of the 8 March 2010 Kovancılar (Elâzığ, Turkey) earthquake (Mw = 6.1). *Geophys. Res. Lett.* **38**, L11304 (2011).
23. Pousse-Beltran, L. et al. The 2020 Mw 6.8 Elâzığ (Turkey) earthquake reveals rupture behavior of the East Anatolian Fault. *Geophys. Res. Lett.* **47**, e2020GL088136 (2020).
24. Konca, A. O. et al. From interseismic deformation with near-repeating earthquakes to co-seismic rupture: a unified view of the 2020 Mw6.8 Sivrice (Elazığ) Eastern Turkey Earthquake. *J. Geophys. Res.: Solid Earth* **126**, e2021JB021830 (2021).
25. Ambraseys, N. N. Temporary seismic quiescence: SE Turkey. *Geophys. J. Int.* **96**, 311–331 (1989).
26. Güvercin, S. E. et al. Active seismotectonics of the East Anatolian Fault. *Geophys. J. Int.* **230**, 50–69 (2022).
27. Duman, T. Y. et al. Paleoseismology of the western Sürgü–Misis fault system: East Anatolian Fault, Turkey. *Mediterr. Geosci. Rev.* **2**, 411–437 (2020).
28. Taymaz, T. et al. Source mechanism and rupture process of the 24 January 2020 Mw 6.7 Doğanyol–Sivrice earthquake obtained from seismological waveform analysis and space geodetic observations on the East Anatolian Fault Zone (Turkey). *Tectonophysics* **804**, 228745 (2021).
29. Melgar, D. et al. Sub- and super-shear ruptures during the 2023 Mw 7.8 and Mw 7.6 earthquake doublet in SE Türkiye. *Seismica*. https://doi.org/10.26443/seismica.v2i3.387 (2023).
30. Güvercin, S. E. Earthquake doublet in Türkiye reveals the complexities of the East Anatolian Fault Zone: insights from aftershock patterns and moment tensor solutions. *Seismol. Res. Lett.* **95**, 664–679 (2024).
31. Provost, F. et al. High-resolution co-seismic fault offsets of the 2023 Türkiye earthquake ruptures using satellite imagery. *Sci. Rep.* **14**, 6834 (2024).
32. Woodcock, N. H. The role of strike-slip fault systems at plate boundaries. *Philos. Trans. R. Soc. A* **317**, 13–29 (1986).
33. Wesnousky, S. G. Seismological and structural evolution of strike-slip faults. *Nature* **335**, 340–343 (1988).
34. Aksu, A. E. et al. Miocene–Quaternary tectonic, kinematic and sedimentary evolution of the eastern Mediterranean Sea: a regional synthesis. *Earth-Sci. Rev.* **220**, 103719 (2021).
35. Çıvgın, B. & Scordilis, E. M. Investigating the consistency of online earthquake catalogs of Turkey and surroundings. *J. Seismol.* **23**, 1255–1278 (2019).
36. Tan, O. et al. The earthquake catalogues for Turkey. *Turkish J. Earth Sci.* **17**, 405–418 (2008).
37. Chen, J. et al. Decoding stress patterns of the 2023 Turkey-Syria earthquake. Under Review. https://doi.org/10.21203/rs.3.rs-2922091/v1 (2024).
38. Taymaz, T. Source parameters of large earthquakes in the East Anatolian Fault Zone (Turkey). *Geophys. J. Int.* **106**, 537–550 (1991).
39. Zoback, M. L. First- and second-order patterns of stress in the lithosphere: the world stress map project. *J. Geophys. Res.* **97**, 11703–11728 (1992).
40. Salditch, L. et al. Earthquake supercycles and long-term fault memory. *Tectonophysics* **774**, 228289 (2020).
41. Ambraseys, N. N. & Jackson, J. A. Faulting associated with historical and recent earthquakes in the Eastern Mediterranean region. *Geophys. J. Int.* **133**, 390–406 (1998).
42. Guidoboni, E. et al. CFTI5Med, the new release of the catalogue of strong earthquakes in Italy and in the Mediterranean area. *Sci. Data* **6**, 80 (2019).
43. Hubert-Ferrari, A. et al. A 3800 yr paleoseismic record (Lake Hazar sediments, eastern Turkey): implications for the East Anatolian Fault seismic cycle. *Earth Planet. Sci. Lett.* **538**, 116152 (2020).
44. Grant, L. B. & Sieh, K. Paleoseismic evidence of clustered earthquakes on the San Andreas Fault in the Carrizo Plain, California. *J. Geophys. Res.* **99**, 6819e6841 (1994).
45. Felzer, K. R. & Brodsky, E. E. Decay of aftershock density with distance indicates triggering by dynamic stress. *Nature* **441**, 735–738 (2006).
46. van der Elst, N. J. & Shaw, B. E. Larger aftershocks happen farther away: nonseparability of magnitude and spatial distributions of aftershocks. *Geophys. Res. Lett.* **42**, 5771–5778 (2015).
47. Wells, D. L. & Coppersmith, K. J. New empirical relationships among magnitude, rupture length, rupture width, rupture area, and surface displacement. *Bull. Seismol. Soc. Am.* **84**, 974–1002 (1994).
48. Guo, H. et al. Seismological indicators of geologically inferred fault maturity. *J. Geophys. Res.: Solid Earth* **128**, e2023JB027096 (2023).
49. Dascher-Cousineau, K. et al. What controls variations in aftershock productivity? *J. Geophys. Res.: Solid Earth* **125**, e2019JB018111 (2020).
50. Collettini, C. et al. Rock and fault rheology explain differences between on fault and distributed seismicity. *Nat. Commun.* **13**, 5627 (2022).
51. Artemieva, I. M. & Shulgin, A. Geodynamics of Anatolia: lithosphere, thermal structure and thickness. *Tectonics* **38**, 4465–4487 (2019).
52. Mia, M. S. et al. Spatio-Temporal clustering of seismicity enabled by off-fault plasticity. *Geophys. Res. Lett.* **49**, e2021GL097601 (2022).
53. Abdelmeguid, M. et al. On the Interplay between distributed bulk plasticity and local fault slip in evolving fault zone complexity. *Authorea*. https://doi.org/10.22541/au.170534677.74205456/v1 (2024).
54. Mia, M. S. et al. The spectrum of fault slip in elastoplastic fault zones. *Earth Planet. Sci. Lett.* **619**, 118310 (2023).
55. Manighetti, I. et al. Earthquake scaling, fault segmentation, and structural maturity. *Earth Planet. Sci. Lett.* **253**, 429–438 (2007).
56. Perrin, C. et al. The shear deformation zone and the smoothing of faults with displacement. *J. Geophys. Res.: Solid Earth* **126**, e2020JB020447 (2021).
57. Perrin, C. et al. Location of largest earthquake slip and fast rupture controlled by along-strike change in fault structural maturity due to fault growth. *J. Geophys. Res.: Solid Earth* **121**, 3666–3685 (2016).
58. Hatem, A. E. et al. Strain localization and evolving kinematic efficiency of initiating strike-slip faults within wet kaolin experiments. *J. Struct. Geol.* **101**, 96–108 (2017).
59. Visage, S. et al. Evolution of the off-fault deformation of strike-slip faults in a sand-box experiment. *Tectonophysics* **847**, 229704 (2023).
60. Howarth, J. D. et al. Spatiotemporal clustering of great earthquakes on a transform fault controlled by geometry. *Nat. Geosci.* **14**, 314–320 (2021).
61. Iezzi, F. et al. Temporal and spatial earthquake clustering revealed through comparison of millennial strain-rates from ^{36}Cl cosmogenic exposure dating and decadal GPS strain-rate. *Sci. Rep.* **11**, 23320 (2021).
62. Mildon, Z. K. et al. Surface faulting earthquake clustering controlled by fault and shear-zone interaction. *Nat. Commun.* **13**, 7126 (2022).
63. Nocquet, J.-M. et al. Supercycle at the Ecuadorian subduction zone revealed after the 2016 Pedernales earthquake. *Nat. Geosci.* **10**, 145–149 (2017).
64. Delvaux, D. & Sperner, B. In *New Insights into Structural Interpretation and Modelling* (ed. Nieuwland, D.) Vol. 212, 75–100 (Geological Society, 2003).
65. Billi, A. et al. Supplementary Information for "Seismic slip channeling along the East Anatolian Fault illuminates long-term supercycle behavior. *Figshare*. https://doi.org/10.6084/m9.figshare.27019849 (2024).

66. GEBCO Compilation Group. GEBCO 2024 Grid. https://doi.org/10.5285/1c44ce99-0a0d-5f4f-e063-7086abc0ea0f (2024).
67. DeMets, C. et al. Geologically current plate motions. *Geophys. J. Int.* **181**, 1–80 (2010).
68. Bletery, Q. et al. Distribution of interseismic coupling along the North and East Anatolian Faults inferred from InSAR and GPS data. *Geophys. Res. Lett.* **47**, e2020GL087775 (2020).
69. Wessel, P. The generic mapping tools version 6. *Geochem. Geophys. Geosyst.* **20**, 5556–5564 (2019).

Acknowledgements

For this work, the authors received only institutional funding from their respective institutions. Funding for open access was provided by Consiglio Nazionale delle Ricerche, IGAG.

Author contributions

All authors conceived the idea of the study that was led by A.B.; B.O., D.P., and C.T. performed analysis of the seismic data with help from F.C., M.C., and M.P.; F.C., M.C., and M.P. performed spatial analysis of seismic and tectonic data with help from A.B., B.O., D.P., and C.T.; F.C., M.C., B.O., D.P., and C.T. processed the preliminary and final images; all authors interpreted and discussed together the results; A.B. wrote the original draft and collected comments from all authors; A.B. reviewed and finalized the manuscript with help from all authors.

Competing interests

The authors declare no competing interests.

Additional information

Supplementary information The online version contains supplementary material available at https://doi.org/10.1038/s41467-024-53234-0.

Correspondence and requests for materials should be addressed to Andrea Billi.

Peer review information *Nature Communications* thanks Mohamed Abdelmeguid, Tuncay Taymaz, Yijun Zhang and the other, anonymous, reviewer(s) for their contribution to the peer review of this work. A peer review file is available.